The design of microfluidic affinity chromatography systems for the separation of bioanalytes

The design of microfluidic affinity chromatography systems for the separation of bioanalytes

Daniel Friedrich[a,**], Colin P. Please[b], Tracy Melvin[a,*]

[a] *Optoelectronics Research Centre, University of Southampton, Highfield, Hampshire, SO17 1BJ, UK*
[b] *School of Mathematics, University of Southampton, Highfield, Hampshire, SO17 1BJ, UK*

Abstract

The analytical (numerical) design of planar microfluidic affinity chromatography devices, which consist of multiple separation lanes and multiple, different surface-immobilised receptor patterns in each lane, is described. The model is based on the analytical solution of the transport-reaction equations in microfluidic systems of low Gratz number and for injection of small analyte plugs. The results reveal a simple approach for the design of microfluidic affinity chromatography devices tailored to the separation of bioanalytes, where receptors with high binding affinity are available. These devices have been designed for bioanalytical applications in mind, most notably for the proteomics field; the results are illustrated with an example using β-Amyloid binding peptides.

Keywords: Affinity chromatography, microfluidic, mathematical modelling, separation, design strategy, β-Amyloid binding peptides

1. Introduction

Efficient separation devices and methods are required for many bioanalytical applications, most notably for proteomic profiling of small samples [1]. Although, there are laboratory-scale methods for the sensitive separation and analysis of protein samples, i.e. capillary electrophoresis coupled with mass spectrometry [2], proteome profiling methods currently requires significant laboratory based effort often requiring several days work. Integration of the different separation, processing and analysis steps into one lab-on-a-chip device would be highly desirable and would offer an approach requiring limited sample handling [3]. Such a lab-on-a-chip format offers the possibility to have many parallel analysis channels, each containing many sequential steps such as enzymatic digestion, multiple separation steps and connection to in-line detection methods [4, 5]. So far some of the necessary component elements, needed for integration within lab-on-a-chip devices for the multiplexed analysis of complex protein mixtures, have been created [6]. However a major 'stumbling block' is the current lack of microfluidic systems for the effective separation of proteins [7].

Protein separation in microfluidic channels, instead of in electrophoresis gels or capillaries, has received much recent interest [8]. The physical properties of microfluidic devices [9] make them attractive for microanalytical assays [10], microchannels for enzymatic digestion (which can be achieved in 5 seconds) [6], affinity capture microfluidic devices [11] as well as aptameric microfluidic systems for purification and enrichment [12], to name a few.

Separation by microfluidic affinity chromatography is based upon highly specific interactions between analytes (often termed as ligands) and immobilised receptors and the retention time of the analytes depends on the strength of the interaction with the immobilised receptors, as illustrated in figure 1 [8]. Examples of immobilised receptors suitable for separation of proteins include antibodies, aptamers or other protein/peptide recognition molecules [13]. These receptors can be easily grafted in patterns to the surface of microfluidic channels using well established conjugation chemistry approaches [14, 15, 16]. Compared to other separation methods, affinity based systems have high specificity and sensitivity which is due to the recognition-binding event. While affinity based separation has been employed in several microfluidic separation systems, these have been limited to single receptor-functionalized gels or bead packed microchannels or even receptor-functionalised nanochannels [4, 10]. However, the format of planar microfluidic devices offers the potential for the incorporation of multiple patterns of different immobilised receptors suitable for the separation of a wider range of analytes, notably for mixtures of analytes which bind with different affinities to different receptors. The need for microfluidic separation systems for the separation of complex mixtures of bioanalytes is well documented [17]. Indeed flow systems which incorporate surface plasmon resonance sensors, such as the Biacore system, provide excellent tools for the identification of high affinity antibody fragments from phage display libraries [18, 19] or for screening of proteins or peptides with antibodies or other binding proteins [20, 21, 22]. For the separation and elution of complex mixtures of proteins a microfluidic affinity chromatography device with patterns of different

*Corresponding author, Tel: +44 23 80596505, Fax: +44 23 80593149, Email: tm@ecs.soton.ac.uk
**Current address: Institute for Materials and Processes, University of Edinburgh, UK

receptors over which the analytes flow and associate-dissociate in a predictable manner is required. So far the tailored design of these systems for the separation of different biomolecules or classes of biomolecules using microfluidic devices with single or multiple patterns of immobilised receptors has been lacking. (We will describe these microfluidic devices with single and multiple patterns of immobilised receptors as simple and multiplex separation systems, from now on.) For such multiplex separation systems to be valuable, tailored design is crucial.

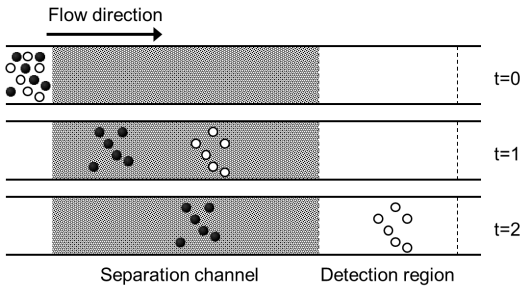

Figure 1: Top view of a simple affinity device for three different times. The receptors (black hatching) specifically interact with the black analytes while they have no affinity for the white analytes. This results in different retention times for the two analytes.

Here the reaction-dispersive model, a model which has been applied extensively for column chromatography applications [23], is used for describing the fluidic and molecular processes in open microfluidic affinity separation systems. This theoretical framework is developed to describe simple and multiplex separation systems.

2. Theoretical model

A theoretical model where both (i) the transport of an analyte plug in a microfluidic channel and (ii) the interaction between the analyte molecules and surface immobilised receptors, is considered. The transport of an analyte plug in the bulk of the microfluidic channel is described by the convection-diffusion equation

$$\frac{\partial A}{\partial t} + \mathbf{u} \cdot \nabla A = D \Delta A \tag{1}$$

where A is the analyte concentration, $\mathbf{u} = (u, v, w)$ is the flow vector and D is the diffusion coefficient [24]. A schematic of the microfluidic channel is shown in figure 2. The association/dissociation of the analyte molecules with the surface immobilised receptor molecules is described by the following reaction scheme

$$A + X \underset{k_d}{\overset{k_a}{\rightleftharpoons}} B \tag{2}$$

where X are the vacant surface immobilised receptors, B are the bound analyte molecules and k_a and k_d are the association and dissociation rates of the bimolecular process. This equation (2) describes the simplest, 1 : 1 analyte-receptor association. It is

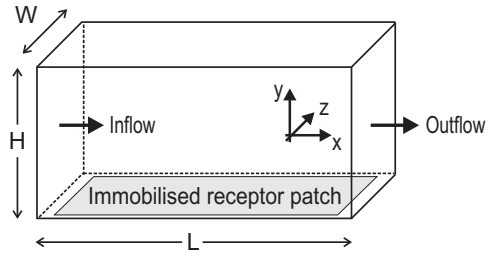

Figure 2: Schematic of the microfluidic channel showing the dimensions and naming conventions.

assumed that the Langmuir isotherm is fulfilled, i.e. monolayer coverage, receptor site equivalence and independence [25]. By the law of mass action, the analyte-receptor association at the immobilised receptor surface (on the receptor patch) can be reformulated into the following differential equation

$$D \frac{\partial A}{\partial y} = \frac{\partial B}{\partial t} = k_a A (X_0 - B) - k_d B \tag{3}$$

where it is assumed that the binding site of the receptor molecules is either vacant or occupied by an analyte molecule so that $B + X = X_0$ where X_0 is the total concentration of surface immobilised receptor molecules. This differential equation (3) describes the dynamics of the analyte association at the immobilised receptor surface. This equation acts as the boundary condition for the differential equation (1) which describes the analyte mass transfer within the microfluidic channel. In contrast to much of the published work [26] this paper is concerned with small analyte plugs. For a short plug in relation to the channel length, $\lambda U \ll L$ where λ is the input time of the analyte plug and U is the average flow velocity.

To gain an insight into the relevance of the physical effects, the governing equations and boundary conditions are nondimensionalised with the following variables: $x = L\tilde{x}$, $y = H\tilde{y}$, $z = W\tilde{z}$, $\mathbf{u} = \left(U, \frac{UH}{L}, \frac{UW}{L}\right)\tilde{\mathbf{u}}$, $A = A_0\tilde{A}$, $X = X_0\tilde{X}$, $B = X_0\tilde{B}$, $t = \frac{L}{U}\tilde{t}$ and $\lambda = \frac{L}{U}\tilde{\lambda}$. Here the tilde indicates the nondimensional variables. The resulting nondimensional system is

$$\tilde{A}_{\tilde{t}} + \tilde{\mathbf{u}} \cdot \nabla \tilde{A} = \mathrm{Gz}^{-1} \left(\frac{H^2}{L^2} \tilde{A}_{\tilde{x}\tilde{x}} + \tilde{A}_{\tilde{y}\tilde{y}} + \frac{H^2}{W^2} \tilde{A}_{\tilde{z}\tilde{z}} \right) \tag{4}$$

$$x, y, z \in [0, 1],$$

$$\mathrm{D_c\,Gz}\, \tilde{B}_{\tilde{t}} = \tilde{A}_{\tilde{y}} = \mathrm{Da} \left(\tilde{A}(1 - \tilde{B}) - \bar{\mathrm{K}}_\mathrm{d}\, \tilde{B} \right) \tag{5}$$

$$x, z \in [0, 1], y = 0.$$

The remaining boundary conditions are (i) no diffusive flux across the outlet, (ii) no flux across channel walls, and (iii) sample injection at the channel inlet. Initially no analyte is in the microfluidic channel ($A = 0$) and all surface immobilised receptor molecules are vacant ($B = 0$). For the ease of readability the tilde atop the nondimensional variables is neglected from now on. The nondimensionalisation reveals four nondi-

mensional numbers:

$$\mathrm{Gz} = \frac{H^2 U}{LD} = \frac{\text{diffusion time}}{\text{convection time}}, \tag{6}$$

$$\mathrm{Da} = \frac{k_a H X_0}{D} = \frac{\text{association rate}}{\text{diffusion rate}}, \tag{7}$$

$$\mathrm{D_c} = \frac{X_0}{A_0 H} = \frac{\text{maximum concentration solid phase}}{\text{maximum concentration mobile phase}}, \tag{8}$$

$$\bar{\mathrm{K}}_\mathrm{d} = \frac{k_d}{k_a A_0} = \frac{\text{dissociation constant}}{\text{analyte concentration}}. \tag{9}$$

The nondimensional numbers are as follows: the Graetz number Gz is a measure of the relative importance of diffusion and convection; the Damköhler number Da relates the rate of diffusion of the analyte molecules toward the immobilised receptor motif to the rate of association between the analyte and surface immobilised receptor molecules on the motif; $\mathrm{D_c}$ is maximum concentration distribution ratio, i.e. the ratio of the number of surface immobilised receptor molecules (as a function of the channel height H) to the number of analyte molecules; the nondimensional dissociation constant $\bar{\mathrm{K}}_\mathrm{d}$ is the dissociation constant $\mathrm{K_d} = k_d/k_a$ scaled with the analyte concentration. For $\bar{\mathrm{K}}_\mathrm{d} \ll 1$ every receptor molecule is occupied by an analyte molecule, in equilibrium while for $\bar{\mathrm{K}}_\mathrm{d} \gg 1$ only a small fraction of the surface immobilised receptor molecules are occupied.

In this paper we consider only shallow and wide rectangular microfluidic channels, i.e. $H/W \to 0$ and $H/L \to 0$ and thus the governing equation (4) in the bulk of the channel is reduced to

$$A_t + u(y) A_x = \mathrm{Gz}^{-1} A_{yy} \tag{10}$$

where the flow profile is parabolic over the height of the channel so that $\mathbf{u} = (u(y), 0, 0)$. Here, we consider only systems at the asymptotic limit $\mathrm{Gz} \ll 1$. This limit is of practical relevance because it ensures that all the analyte molecules in the plug approach the surface immobilised receptors - a requirement applicable to many other microfluidic systems [27]. Previously we have shown that at this asymptotic limit the equation (10) can be integrated over the height of the channel and reduced to a 1D equation; this describes the convection of the analyte plug and the reaction between the analyte molecules and surface immobilised receptor molecules [24]. Equations (4)-(5) are thus reduced to

$$\frac{\partial A}{\partial t} + \frac{\partial A}{\partial x} = -\zeta(A(1-B) - \bar{\mathrm{K}}_\mathrm{d} B), \tag{11}$$

$$\frac{\partial B}{\partial t} = \frac{\zeta}{\mathrm{D_c}}(A(1-B) - \bar{\mathrm{K}}_\mathrm{d} B) \tag{12}$$

where ζ is the nondimensional reaction/convection number

$$\zeta = \frac{\mathrm{Da}}{\mathrm{Gz}} = \frac{k_a L X_0}{HU} = \frac{\text{binding rate}}{\text{convection rate}} \tag{13}$$

The boundary and initial conditions for the differential equations (11) and (12) are given by an initially empty system ($A = B = 0$) and a fixed analyte concentration at the inlet

$$A(x=0,t) = \delta(t) \qquad , t \geq 0, \tag{14}$$

where the Dirac delta function δ specifies the analyte input. The binding/convection number ζ is the ratio between the binding rate and the convection rate. For a small binding/convection number ($\zeta \ll 1$) the transport is 'binding limited', i.e. the association is the rate limiting step, while for a large binding/convection number ($\zeta \gg 1$) the system becomes 'convection limited'.

For the case where the number of analyte molecules is far lower than the number of surface immobilised receptor molecules, $\mathrm{D_c} \gg 1$, the time derivative of the nondimensional bound concentration B_t in equation (12) will approach zero. Therefore the nondimensional bound concentration B will remain close to the initial value of 0 and can thus be removed from the association term in equation (11) and (12). This results in the transformation of the second order kinetics into first order kinetics. The resulting linear differential equations can be solved analytically by the Laplace transform method [28]

$$A(x,t) = e^{-\zeta x}\hat{\mathrm{H}}(t-x)\delta(x-t) + e^{-\zeta x - \frac{\zeta \bar{K}_d}{\mathrm{D_c}}(t-x)} \sqrt{\frac{\zeta^2 \bar{K}_d x}{\mathrm{D_c}(t-x)}} I_1(2\sqrt{\zeta^2 \bar{K}_d x(t-x)/\mathrm{D_c}})(1-\hat{\mathrm{H}}(x-t)), \tag{15}$$

$$B(x,t) = \frac{\zeta}{\mathrm{D_c}} e^{-\zeta x} e^{-\zeta \bar{K}_d (t-x)/\mathrm{D_c}} I_0(2\sqrt{\zeta^2 \bar{K}_d x(t-x)/\mathrm{D_c}})(1-\hat{\mathrm{H}}(x-t)), \tag{16}$$

where $\hat{\mathrm{H}}$ is the Heaviside step function.

The first term in equation (15) is a description of how the (initial) analyte plug travels down the channel and associates with the surface immobilised receptors. The second term describes the 'secondary plug' which develops for $t > x$. This analyte plug consists of analyte which has previously been bound to the surface immobilised receptors (and subsequently dissociated). Figure 3 shows the distribution of unbound analyte along the channel calculated from equation (15). It can be inferred

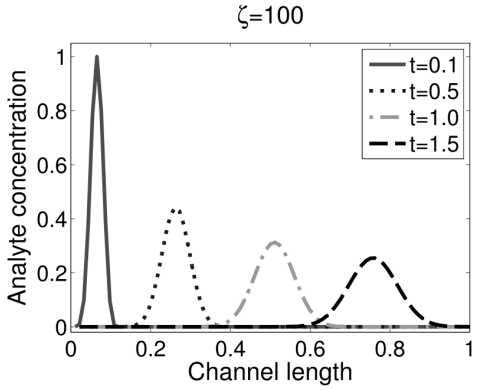

Figure 3: Plot of the unbound analyte concentration A calculated from equation (15) along the length of the channel for various times t. The plots are normalised with the maximum analyte concentration for $t = 0.1$. Parameters: $\zeta = 100$, $\mathrm{D_c} = 10$, $\bar{K}_d = 10$

that the analyte plug disperses and moves slower than the mobile phase flow velocity ($u = 1$), which is due to the adsorption/desorption of the analyte molecules at the immobilised re-

ceptor patch. Expressions describing the dispersion and retention of the analyte molecules are derived in the next section.

3. Derivation of expressions for the analyte plug velocity and plug dispersion

Assuming fast adsorption ($\zeta \gg 1$), the first term of equation (15) quickly approaches zero and only the second term, which is zero for $t < x$, has to be considered. For $t > x$ the variable $w = 2\sqrt{\zeta^2 \bar{\mathrm{K}}_\mathrm{d}\, x(t-x)/\,\mathrm{D_c}} \gg 1$ and the Bessel function can therefore be approximated using $I_1(w) \approx \frac{e^w}{\sqrt{2\pi w}}$ [29]. Thus equation (15) can be approximated by

$$A \approx \sqrt{\frac{\zeta\sqrt{\bar{\mathrm{K}}_\mathrm{d}}}{4\pi\sqrt{\mathrm{D_c}}}}\sqrt{\frac{\sqrt{x}}{(t-x)^{3/2}}} \exp\left(2\sqrt{\zeta^2 \bar{\mathrm{K}}_\mathrm{d}\, x(t-x)/\,\mathrm{D_c}} - \zeta x + \zeta\,\bar{\mathrm{K}}_\mathrm{d}(x-t)/\,\mathrm{D_c}\right). \tag{17}$$

In order to establish where the maximum concentration of the analyte at a specific time is located within the channel equation (17) is applied. By elucidating the position of the maximum concentration of the analyte as a function of time the plug velocity can be determined. This maximum occurs where the first derivative is zero and gives the velocity u_p of the peak concentration of the analyte plug as

$$u_p = \frac{x}{t} = \frac{1}{1 + \mathrm{D_c}\,/\,\bar{\mathrm{K}}_\mathrm{d}} = \frac{1}{1 + \frac{k_a X_0}{k_d H}}. \tag{18}$$

Here the ratio of the numbers of surface immobilised receptors to analyte molecules $\mathrm{D_c}$ and the nondimensional dissociation constant $\bar{\mathrm{K}}_\mathrm{d}$ defines the nondimensional retention factor

$$\mathrm{k} = \frac{\mathrm{D_c}}{\bar{\mathrm{K}}_\mathrm{d}} = \frac{k_a X_0}{k_d H} \tag{19}$$

which is a measure for the retention of an analyte plug in microfluidic affinity separation systems. For $\mathrm{k} \ll 1$ the retention of the analyte plug is low and the plug velocity approaches the mobile phase velocity. For $\mathrm{k} \gg 1$ the retention of the analyte plug is high and the plug velocity reaches zero.

Figure 3 shows that as the analyte plug moves along the channel it broadens; this can be described as an approximation of equation (17) as a Gaussian located at the analyte peak. For the Gaussian function the full width at half maximum (FWHM) is related to the variance, σ^2, and given by $\mathrm{FWHM} = 2\sqrt{2\log 2}\sigma$. At the location of the maximum concentration of the analyte plug, the variance σ^2 is proportional to the second derivative of the exponential part from equation (17) and thus

$$\sigma^2 = t\frac{2\,\mathrm{k}^2}{\zeta(1+\mathrm{k})^3} = x\frac{2\,\mathrm{k}^2}{\zeta(1+\mathrm{k})^2}. \tag{20}$$

This shows that the standard deviation σ, and therefore the plug dispersion, is dependent on $\sqrt{t}$ and the nondimensional device parameters k and ζ.

4. Design framework

The multiplex affinity chromatography separation device concept is shown in figure 4; this is a microfluidic device with a number of differently sized receptor patches in adjoining lanes. Whilst conventional affinity chromatography systems are simply allowing for injection of a mixture of analytes over a single (affinity) receptor matrix, the potential advantage of microfluidic affinity chromatography systems is that a mixture of analytes could be separated over different sized patterns of multiple, different receptors immobilised on the surface, and thus offer the potential for the multiple separations to be done simultaneously. To achieve this the length and type of the receptor patches are designed so that each lane separates a different range of analytes; for example, lane 1 could be designed to retain one class of proteins while the other lanes are design for different classes of proteins. Thus by designing a separation device with several lanes which each separate a certain range of analytes multiple separations can be performed simultaneously; that is multiple analytes are co-eluted at the same time but on different lanes.

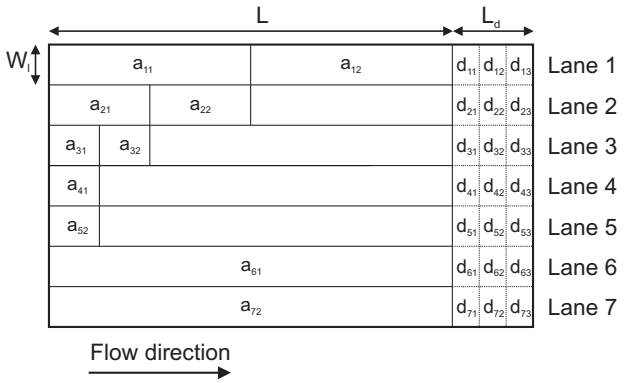

Figure 4: Top view of the proposed separation device. Shown are 7 separation lanes with patches of varying length and immobilised with two different receptors as well as the detection region L_d. The receptor patches are immobilised with the receptors a_{*1} and a_{*2} and have the length a_{ij}.

4.1. Channel design

The receptor patches in each lane i are functionalised with different receptor molecules j. A sample plug, containing analytes, m, is injected from the left and flows over all the lanes through the separation channel with length L. The length a_{ij} of the receptor patches is determined to achieve an optimal separation of the target analytes, i.e. all analytes are separated in at least one lane. The analytes are eluted to the detection region L_d; this is envisaged to be a 'conceptual' structure suitable for ordered elution, identification and quantification of each of the analytes from each lane. The analyte mixture m is proposed to reach the detection region L_d of each of the different lanes such that the detection region L_d for each lane i contains differently separated analytes after a set elution time. (The detector design is not considered in this paper, but it is envisaged that this could

be a structure suitable for mass spectrometry analysis (i.e. matrix assisted laser desorption/ionisation)).

The time of elution of each analyte relative to a blank sample is given by the retention time. The retention time of each analyte over each receptor patch can be calculated from the analytical expression of the plug velocity (18) and is given through

$$t_{ijm} = \frac{\mathrm{a}_{ij}}{(u_p)_{jm}} - \mathrm{a}_{ij} = \mathrm{a}_{ij}(1 + \mathrm{k}_{jm}) - \mathrm{a}_{ij} = \mathrm{a}_{ij}\,\mathrm{k}_{jm} \tag{21}$$

(using the no-summation convention). All variables here are nondimensional and derived through the nondimensionalisations: $\mathrm{a}_{ij} = \frac{\bar{a}_{ij}}{L}$, $t = \frac{\bar{t}U}{L}$, $u = \frac{\bar{u}}{U}$ and $L_p = \frac{\bar{L}_p}{L}$ where the bar indicates the dimensional variables. Thus to get the total retention time of the analyte molecules on a lane, the sum of all receptor patches within the lane must be considered

$$t_{im} = \mathrm{a}_{i1}\,\mathrm{k}_{1m} + \mathrm{a}_{i2}\,\mathrm{k}_{2m} + \mathrm{a}_{i3}\,\mathrm{k}_{3m} + \ldots \tag{22}$$

Extending this expression for multiple patches, lanes and analytes results in the following matrix description for the retention time

$$\begin{pmatrix} \mathrm{a}_{11} & \ldots & \mathrm{a}_{1J} \\ \mathrm{a}_{21} & \ldots & \mathrm{a}_{2J} \\ \vdots & \ddots & \vdots \\ \mathrm{a}_{I1} & \ldots & \mathrm{a}_{IJ} \end{pmatrix} \begin{pmatrix} \mathrm{k}_{11} & \ldots & \mathrm{k}_{1M} \\ \mathrm{k}_{21} & \ldots & \mathrm{k}_{2M} \\ \vdots & \ddots & \vdots \\ \mathrm{k}_{J1} & \ldots & \mathrm{k}_{JM} \end{pmatrix} = \begin{pmatrix} t_{11} & \ldots & t_{1M} \\ t_{21} & \ldots & t_{2M} \\ \vdots & \ddots & \vdots \\ t_{I1} & \ldots & t_{IM} \end{pmatrix} \tag{23}$$

where I, J and M are the total number of lanes, receptor patches and analytes, respectively.

The nondimensional retention times in the matrix (23) can be directly related to the separation of different analytes. For example, the separation between the analyte peaks of the two analytes m and l on lane i is given by $d_{iml} = |t_{im} - t_{il}|$. Thus the retention time matrix (23) is used in section 4.2 to design a separation system so that the widest range of retention factors falls into the detection region L_d.

However, first the channel dimensions have to be specified. The values for the flow velocity U, minimal receptor patch length $L_p = \min(\mathrm{a}_{ij})$, separation channel length $L = \max(\mathrm{a}_{ij})$ and the lane width W_l must fulfil the following conditions so that the model from section 3 is valid:

$$\zeta = \frac{k_a L_p X_0}{HU} > 20, \tag{24}$$

$$Gz = \frac{H^2 U}{L_p D} < 1, \tag{25}$$

$$x_d \sim \sqrt{\frac{2DL}{U}} < W_l. \tag{26}$$

It will be shown in section 4.2 that the ratio r_L of the maximal patch length L, and minimal patch length L_p, is directly proportional to the ratio of the maximal retention factor k_{max}, and minimal retention factor k_{min}, that the channel can separate; thus the channel should be designed to maximise this ratio. While the ratio r_L is independent of the flow velocity, U, it is inversely proportional to the channel height, H, which should be as small as possible. It has been shown that open microfluidic channels with a height less than $10\,\mu$m have higher separation efficiencies than packed microfluidic channels for liquid chromatography applications [30]. Thus a channel height of $5\,\mu$m is a good compromise between separation efficiency and ease of fabrication of the microfluidic channel. Equation (26) describes the cross lane diffusion: once $x_d \sim W_l$ the cross lane diffusion becomes significant.

For a lane of width $W_l = 200\,\mu$m, a diffusion coefficient $D = 5 \times 10^{-11}\,\mathrm{m^2\,s^{-1}}$, an association rate constant $k_a = 10^5\,\mathrm{M^{-1}\,s^{-1}}$ and a surface immobilised receptor concentration $X_0 = 10^{-8}\,\mathrm{mol\,m^{-2}}$ a separation factor of $L/L_p = 4$ can be calculated by rearranging equations (24) and (26) to L_p and L, respectively.

4.2. Patch design for a single type of receptor molecules

The design of systems with only one type of surface immobilised receptor molecules in each lane ($J = 1$), but where the analytes introduced have different retention factors, is now described.

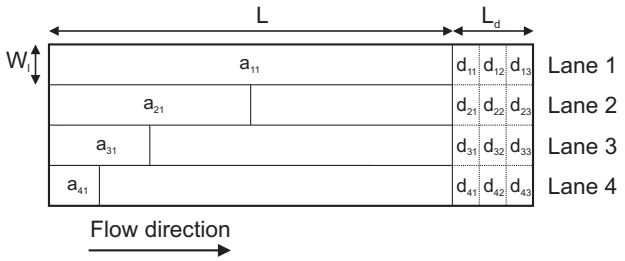

Figure 5: Top view of a separation device with one type of receptor molecules and a separation factor of $\alpha = 2$.

Lane 1 (as illustrated in figure 5) with a receptor patch with the maximal patch length $\mathrm{a}_{11} = 1$ is first considered. This lane is best suited for the separation and subsequent detection of the analyte with the smallest retention factor $\mathrm{k}_{1(min)}$, as shown by equation (22). This analyte is eluted first and thus the system is designed so that it is detected at the end of the detection region L_d. Consequently, in each lane i the analyte with the lowest retention factor $\mathrm{k}_{i(min)}$ is detected at the end of the detection region and the analyte with the highest retention factor $\mathrm{k}_{i(max)}$ at the beginning. Thus the retention time $t_d = \mathrm{a}_{11}\,\mathrm{k}_{1(min)}$ plus the time required to reach the end of the detection region L_d allows the calculation of the maximal retention factor $\mathrm{k}_{1(max)}$ which can be detected in lane 1

$$\mathrm{k}_{1(max)} = \frac{t_d + L_d}{\mathrm{a}_{11}} = \mathrm{k}_{1(min)} + \frac{L_d}{\mathrm{a}_{11}}. \tag{27}$$

In order to cover the full range of relative retention factors, the maximal retention factor of one lane i is set to be equal to the minimal retention factor of the next lane $i+1$, i.e. $\mathrm{k}_{i+1(min)} = \mathrm{k}_{i(max)}$. With this condition the following equation for the patch a_{21} follows

$$\mathrm{a}_{21}\,\mathrm{k}_{2(min)} = \mathrm{a}_{21}\,\mathrm{k}_{1(max)} = t_d = \mathrm{a}_{11}\,\mathrm{k}_{1(min)} \tag{28}$$

Since $t_d = \mathrm{a}_{11}\,\mathrm{k}_{1(min)}$ is constant this leads to the definition of the lane separation factor

$$\alpha = \frac{\mathrm{a}_{i,1}}{\mathrm{a}_{i+1,1}} = \frac{\mathrm{k}_{i(max)}}{\mathrm{k}_{i(min)}} = 1 + \frac{L_d}{\mathrm{a}_{i1}\,\mathrm{k}_{i(min)}} = 1 + \frac{L_d}{t_d}. \tag{29}$$

From equations (28) and (29), simple expressions for the minimal and maximal retention factor of lane i as well as for the patch length a_{i1} in terms of the minimal retention factor $\mathrm{k}_{1(min)}$ and the separation factor α, are obtained.

$$\mathrm{k}_{i(min)} = \alpha^{i-1}\,\mathrm{k}_{1(min)}, \tag{30}$$

$$\mathrm{k}_{i(max)} = \alpha^{i}\,\mathrm{k}_{1(min)}, \tag{31}$$

$$\mathrm{a}_{i1} = \mathrm{a}_{11}\,\alpha^{1-i}. \tag{32}$$

By using these expressions the patch lengths $\mathrm{a}_{21}, \ldots, \mathrm{a}_{I1}$ can be iteratively calculated starting from the maximal patch length $\mathrm{a}_{11} = 1$. Here and from now on I is the total number of lanes required for a system containing a single type of receptor patch and $\mathrm{a}_{min} = L_p$ is chosen so that $\mathrm{a}_{min} = \mathrm{a}_{11}\,\alpha^{1-I}$. The resulting patch design for $I = 4$ and $\alpha = 2$ is shown in figure 5 where the patch length decreases exponentially from L to $L/2$ to $L/4$ to $L/8$. The corresponding retention factors increase exponentially: $\mathrm{k}_{1(min)} = 2^{-1}\,\mathrm{k}_{1(max)} = 2^{-1}\,\mathrm{k}_{2(mim)} = 2^{-2}\,\mathrm{k}_{2(max)} = 2^{-2}\,\mathrm{k}_{3(mim)} = 2^{-3}\,\mathrm{k}_{3(max)} = 2^{-3}\,\mathrm{k}_{4(mim)} = 2^{-4}\,\mathrm{k}_{4(max)}$.

4.3. Patch design for multiple types of receptor molecules

Microfluidic affinity chromatography systems with patches of a single receptor type are only suitable for separating analytes which bind to this receptor. In order to apply microfluidic affinity chromatography systems for the separation of analytes which bind to different receptors, receptor patches with different types of receptor molecules are required. Thus lanes containing two types of immobilised receptor molecules ($J = 2$) patterned as two patches in series on the surface of the microfluidic channel (see figure 4), are now considered.

The optimal receptor patch configuration of a multiplex microfluidic affinity chromatography device patterned with two different receptor molecules can be derived graphically as shown in figure 6. The y and x axis show the relative retention factor, i.e. relative to the smallest retention factor, with respect to the receptor molecules 1 and 2, respectively; thus each position on this graph corresponds to an analyte with a specific combination of retention factors with respect to the two receptor molecules.

Here, the graphical derivation is done by considering the smallest possible patch length first; for the example in figure 6 this is $\mathrm{a}_{max}\,\alpha^{-3}$. Two patches, one for receptor 1 and one for receptor 2, with the smallest possible patch length are placed in lane 3, see the schematic in figure 4. This lane separates analytes with retention factors that fall in the shaded area 3 in figure 6. Lane 2 is patterned with two patches of length $\mathrm{a}_{max}\,\alpha^{-2}$ and separates analytes with retention factors that fall in the shaded area 2. By iteratively assessing longer patch lengths the configuration shown in the first three lanes of figure 4 is reached; this configuration corresponds to the detection regions shown in figure 6.

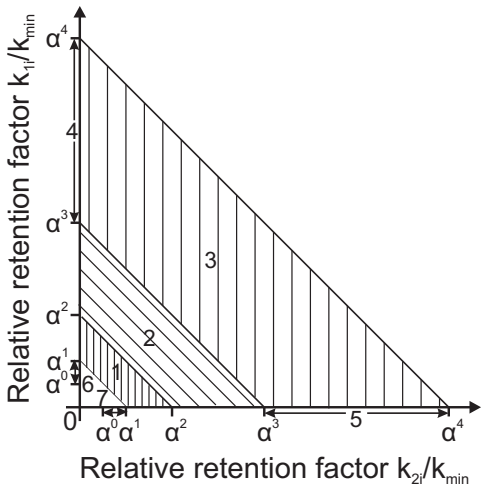

Figure 6: Plot over the separation factor of the two immobilised receptors used for the design of two patch separation systems: the shaded area for each lane 1 to 3 indicates the combination of k_{1i} and k_{2i} which this dual-patch lane can separate (see figure 4). The additional single-patch lanes 4 to 7 shown in figure 4 are indicated by arrows along the axes. k_{min} is the smallest retention factor the system can separate and the separation factor is $\alpha = 2$.

From figure 6 it can be seen that analytes with relative retention factors which fall below the area covered by the shaded region 1 or above shaded region 3 are not separated by any of the dual patch lanes, 1, 2 or 3. In order to separate analytes with relative retention factors not covered, four additional lanes patterned with single receptors could be used, as shown schematically in figure 4 and indicated by the arrows along the axes in figure 6, lanes $4 - 7$. For instance, the receptor patch shown in lane 4 is suitable for the separation of analytes with relative retention factor k_{1i}/k_{min} between α^3 and α^4 as illustrated by the range labelled with the arrow 4, and the receptor patch in lane 6 is suitable for the separation of analytes with relative retention factor k_{1i}/k_{min} between α^0 and α^1 as illustrated by the range identified by the arrow 6, in figure 6. The combination of dual and single patch lanes provides a system where analytes with different retention factors have the potential to be separated on at least one of the lanes.

4.4. Analyte separation

Most analytes which are recognised by either or both immobilised receptors in the multiplex separation device with dual patches (described above) can be separated. This is now considered using the schematic shown in figure 7. Here the analytes A_1 and A_3 have the same retention factor for the immobilised receptor molecules 1; thus the two analytes are not separated from each other by the single-patch lane as indicated by the continuous lines ($\alpha^1\,\mathrm{k}_{min}$ and $\alpha^2\,\mathrm{k}_{min}$). Whereas, these analytes can be separated by a dual-patch lane with retention factor values bounded by the dashed lines in figure 7.

Not all dual-patch system designs separate all analyte pairs. One example is illustrated schematically in figure 7, where the relative retention factors have values which fall on or are on a line parallel to one of the region boundaries, as shown by ana-

lytes A_1 and $\bar{A}_1$. Although these analytes have different affinities for the two receptor molecules they will arrive at the detection region L_d at the same time and thus will not be separated. In order to separate specific analytes with known retention factors it is necessary to design dual receptor patches accordingly. Thus the design of simple (one lane) affinity chromatography microfluidic systems tailored for the separation of two different analytes $A_1 = (\mathrm{k}_{11}, \mathrm{k}_{21})$ and $A_2 = (\mathrm{k}_{12}, \mathrm{k}_{22})$, is now described. Using figure 7 for illustration, this hypothetical case is plotted (see points labelled A_1 and A_2). Without loss of generality it is assumed that $\mathrm{k}_{11} \geq \mathrm{k}_{12}$.

First a channel with a single immobilised receptor patch (J=1) is considered. The choice of single patch dimension is one where the difference in retention time between the peaks of two analytes is maximised. This case is given where the analyte with the larger relative retention factor (i.e. A_1) is on the upper boundary of the separation range. Using figure 7 for illustration, this case is shown by the continuous lines. The patch length for this case is given by

$$\mathrm{a}_1 = \frac{t_d + L_d}{\mathrm{k}_{11}} \tag{33}$$

and thus the maximal peak separation distance for a single-patch system according to the retention time matrix (23) is given by

$$d_s = (\mathrm{k}_{11} - \mathrm{k}_{12})\frac{t_d + L_d}{\mathrm{k}_{11}} = \left(1 - \frac{\mathrm{k}_{12}}{\mathrm{k}_{11}}\right)(t_d + L_d). \tag{34}$$

This single-patch separation distance is now compared to the optimal dual-patch separation distance. Again, the choice of dual-patch dimensions is one where the difference in retention time between the peaks of the two analytes is maximised by placing the analyte with the larger retention factor on the upper boundary of the separation range. The boundaries for the separation range are defined by plotting these perpendicular to the line between the points for the two analytes A_1 and A_2, these are shown as dashed lines in the figure 7. The example shown here corresponds to two patches of different lengths $\mathrm{a}_{11} \neq \mathrm{a}_{12}$. Due

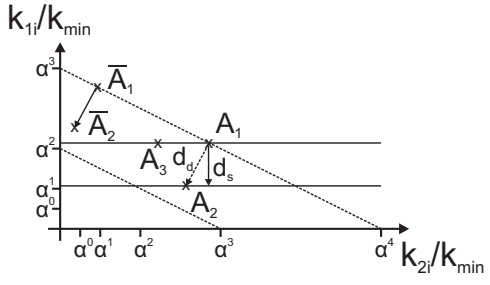

Figure 7: Diagram showing the difference in peak separation distance for single-patch and dual-patch setups for the analytes A_1 and A_2. The analytes $\bar{A}_1$ and $\bar{A}_2$ are shifted from the analytes A_1 and A_2 parallel to the dual-patch boundary. The analytes A_1 and A_3 are eluted at the same time on the single-patch lane but at different times on the dual-patch lane.

to the constraint that the patches and retention factors have to be positive this configuration can only be achieved if $\mathrm{k}_{11} \geq \mathrm{k}_{12}$ and $\mathrm{k}_{21} \geq \mathrm{k}_{22}$; the retention factors of the two analytes are linked by $\mathrm{k}_{i2} = \mathrm{k}_{i1} - \epsilon_i$ where ϵ_1 and ϵ_2 are positive constants. These two constants ϵ_1 and ϵ_2 define the normal to the separation region boundary and are proportional to the patch widths $\mathrm{a}_{11} = c\epsilon_1$ and $\mathrm{a}_{12} = c\epsilon_2$ with a positive constant c which can be determined by using the equation

$$\mathrm{a}_{11}\,\mathrm{k}_{11} + \mathrm{a}_{12}\,\mathrm{k}_{21} = c(\epsilon_1\,\mathrm{k}_{11} + \epsilon_2\,\mathrm{k}_{21}) = t_d + L_d. \tag{35}$$

With the patch widths a_{11} and a_{12} the maximal peak separation distance can be calculated to be

$$d_d = \mathrm{a}_{11}(\mathrm{k}_{11} - \mathrm{k}_{12}) + \mathrm{a}_{12}(\mathrm{k}_{21} - \mathrm{k}_{22}) = c(\epsilon_1^2 + \epsilon_2^2). \tag{36}$$

From this it follows that the peak separation distance between A_1 and A_2 is equal to the peak separation distance between $\bar{A}_1$ and $\bar{A}_2$ in the dual-patch lane setup in figure 7.

Now the maximal dual-patch peak separation d_d is compared with the maximal single-patch peak separation d_s which is dependent on the two analytes in the following way

$$d_{s1} = (\mathrm{k}_{11} - \mathrm{k}_{12})\frac{t_d + L_d}{\mathrm{k}_{11}} = \epsilon_1\frac{t_d + L_d}{\mathrm{k}_{11}}, \qquad \frac{\epsilon_1}{\mathrm{k}_{11}} \geq \frac{\epsilon_2}{\mathrm{k}_{21}}, \tag{37}$$

$$d_{s2} = (\mathrm{k}_{21} - \mathrm{k}_{22})\frac{t_d + L_d}{\mathrm{k}_{21}} = \epsilon_2\frac{t_d + L_d}{\mathrm{k}_{21}}, \qquad \text{otherwise.} \tag{38}$$

Assuming $d_d \geq d_{s1}$ it follows that $\frac{\epsilon_1}{\mathrm{k}_{11}} \leq \frac{\epsilon_2}{\mathrm{k}_{21}}$. Using this it can be shown that $d_{s1} \leq d_d \leq d_{s2}$ so that the dual-patch peak separation distance can never be greater than the maximal single-patch peak separation distance. This result is shown schematically in figure 7: for the single-patch lane the analyte A_1 is detected at the beginning of the detection region and the analyte A_2 at the end while for the dual-patch lane the analyte A_1 is detected at the beginning of the detection region and the analyte A_2 between the beginning and end of the detection region. This result can be extend to lanes with more patches and will give a similar result.

To get a useful measure of the separation of two analyte plugs the width of the two plugs has to be taken into account. The plug separation for two analytes A_j and A_l on lane i is given by

$$S_{ijl} = \frac{2|t_{ij} - t_{il}|}{w_{ij} + w_{il}} \tag{39}$$

where w_{ij} and w_{il} are the FWHM of the analyte plugs. Here it is assumed that the analyte plugs are symmetrical, in agreement with the results from figure 3 where the analyte plug can be considered as a Gaussian distribution with variance σ^2. For a linear system the total variance of the analyte plug is the sum of the variance due to adsorption/desorption, given by equation (20), and due to axial dispersion over the various receptor patches [31]. The axial dispersion in pressure driven flow can be described by an effective diffusion coefficient $\tilde{D}$ [32]. The plug width, i.e. the total variance over the patch, at the end of each receptor patch has to be multiplied with the ratio of the plug velocities over this receptor patch and the next receptor patch. The reason for this is that the plug velocity at the patch boundary changes and thus the analyte plug is either 'stretched' or 'compressed' by the change in velocity. Combining these

effects gives the total FWHM of the analyte A_k at the end of lane i

$$w_{ij} = 2\sqrt{2\log 2} \sqrt{(\sigma^2_{i1\,j} + 2\,\mathrm{a}_{i1}\,\tilde{D})\frac{(1+\mathrm{k}_{i2})^2}{(1+\mathrm{k}_{i1})^2} + \cdots + (\sigma^2_{im\,j} + 2\,\mathrm{a}_{im}\,\tilde{D})\frac{(1+\mathrm{k}_{im+1})^2}{(1+\mathrm{k}_{im})^2}} \quad (40)$$

where m is the number of receptor patches in lane i. This allows the calculation of the separation S_{ijl} of the two analytes A_j and A_l on lane i.

5. Application

5.1. Validation

The governing equations derived in this paper can now be used to design microfluidic affinity separation systems for the multiplexed separation of multiple analytes. An example for the separation of a sample plug containing two analytes with different affinities for the receptor molecules is illustrated in figure 8. The two analytes were introduced at the same time as a mixed sample plug onto a one-patch system with $\mathrm{a}_{11} = 1$. The relative error between the peak separation distance and the numerical simulation is less than 1%. Furthermore, the relative error between the FWHM predicted by equation (40) and the FWHM from the numerical simulation is below 6%. This error is due to the difference in initial plug width between the analytical and numerical solution. This shows that the derived equations are a good starting point for the design of a microfluidic affinity chromatography system.

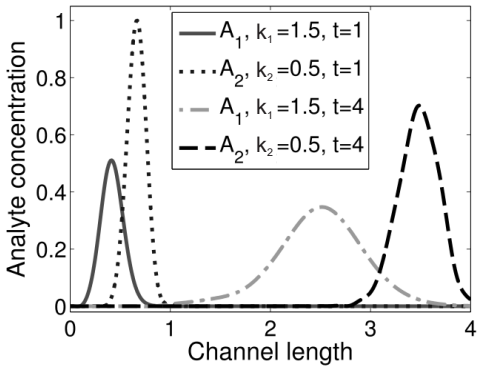

Figure 8: Numerical simulation of the concentration distribution of two analytes A_1 and A_2 with different retention factors $\mathrm{k}_1 = 1.5$ and $\mathrm{k}_2 = 0.5$. Parameter: $\mathrm{a}_{11} = 1$, $\mathrm{Gz} = 0.05$, $\mathrm{D_c} = 250$, $\lambda = 0.05$, $\zeta = 50$

5.2. Design of a microfluidic chromatography system based upon reported experimental data

The approach developed so far allows for the design of microfluidic affinity chromatography systems and we now illustrate this using the experimental data of Cairo *et al*. [20]. As reported, a range of β-Amyloid binding peptides have been evaluated using a surface plasmon resonance sensor and these have dissociation constants in the range of 37 to 1300 μM; giving a ratio of around 35 between the strongest and weakest peptide [20]. To increase the range of further possible β-Amyloid binding peptides (not reported by Cairo *et al*.) we chose to design the system with a lane separation factor $\alpha = 2$ with six lanes: giving a separation factor of $2^6 = 64$. This allows for the separation of analytes with dissociation constants between 30 and 1920 μM. The designed system will be similar to figure 5 with two additional lanes: lane 5 with a patch of length $a_{51} = 0.5a_{41}$ and lane 6 with a patch of length $a_{61} = 0.25a_{41}$. So the system is designed so that mixture is introduced to all the lanes concurrently and then the different analytes in the mixture elute concurrently on the detection region following each lane (see figure 5). The total elution time is chosen so that an analyte with the maximal dissociation constant is at the end of the detection region in lane 1. Table 1 shows the dissociation constants and our choice of lanes for the separation of the peptides (and compound number) reported by Cairo *et al*. [20]. Clearly peptides which have dissociation constants within error of each other might not be separated, but for the purposes of this study the reported standard error of the data of Cairo *et al*. is not considered.

Lane	K_d Range	Compound Number	Sequence	Dissociation Constant (K_d) (μM)	Standard Error (±)
1	960-1920	hypothetical	n.a.	1600	
		18	KLVFFEEEKKK	1300	600
2	480-960				
3	240-480	22	KKKKKK	400	200
		19	KLVFFEKEKEK	300	160
4	120-240	16	KKKKLVFF	180	80
5	60-120	17	KLVFFKKKEEE	90	10
		15	KLVFFKK	80	60
		24	KLVFWKKKKKK	65	10
6	30-60	13	KLVFFKKKKKK	40	10
		21	KLVFFRRRRRR	40	9
		23	KLVWWKKKKKK	40	10
		25	Congo red	38	8
		14	KLVFFKKKK	37	5

Table 1: Separation lanes for β-Amyloid binding peptides with dissociation constants (K_d). The values for the dissociation constants, standard errors and compound numbers are as previously reported by Cairo *et al*. [20]

Starting from a minimal dissociation constant $K_{d,min} = 30\,\mu$M the maximal dissociation constant is $K_{d,max} = 64K_{d,min}$. Thus the minimal and maximal retention factors (eq. (19)) are $k_{min} = 0.094$ and $k_{max} = 6$, respectively. For the lane width, diffusion coefficient and association rate constant, the same parameter values as in section 4.1 are used; these values and the other design parameters are given in table 2. The surface immobilised receptor concentration used in the study of Cairo *et al*. is estimated from the response units (RU) of the immobilisation of the ligand and the molecular weight; this equates to $X_0 = 9\times10^{-7}\,\mathrm{mol\,m^{-2}}$. The system parameters such as channel length, flow velocity and minimal patch length are now determined using equations (24)-(26) and are given in table 2. The first two equations place a limit on the ratio L_p/U. By arbitrarily choosing that the minimal patch length is equal to the lane width, i.e. $L_p = W_l$, the inequalities (24)-(25) are fulfilled for $U = 0.1\,\mathrm{mm\,s^{-1}}$. The last inequality places a limit on the channel length: $L < 0.04\,\mathrm{mm}$ and thus provides a maximum

separation factor of $L/L_p = 200$. With the proposed separation factor the channel length is given as $L = 32L_p = 6.4\,\text{mm}$. To

Parameter	Label	Value	Units
Lane separation factor	α	2	
Analyte concentration	A_0	50	μM
Diffusion coefficient	D	5×10^{-11}	$m^2\,s^{-1}$
Channel height	H	5	μm
Association rate constant	k_a	10^5	$M^{-1}\,s^{-1}$
Minimal retention factor	k_{min}	0.094	
Maximal retention factor	k_{max}	6	
Minimal dissociation constant	$K_{d,min}$	30	μM
Maximal dissociation constant	$K_{d,max}$	1920	μM
Channel length	L	6.4	mm
Detection region length	L_d	0.6	mm
Minimal patch length	L_p	0.2	mm
Elution time	t	76	s
Average flow velocity	U	0.1	$mm\,s^{-1}$
Lane width	W_l	0.2	mm
Surface receptor concentration	X_0	9×10^{-7}	$mol\,m^{-2}$

Table 2: Parameters for the single-patch sensor of immobilized β-Amyloid

obtain a lane separation factor equal to 2 the nondimensional detection region length is set equal to the nondimensional retention time; thus the dimensional detection region length is equal to the minimal retention factor times the channel length: $L_d = k_{min}L = 0.094 \times 6.4\,\text{mm} = 0.6016\,\text{mm}$. The analyte concentration A_0 is chosen so that the concentration distribution ratio (eq. (8)) is larger than 1.

The peak separation between two analytes in the detection region is $0.625\,\mu$m per μM difference in the dissociation constants on lane 1, $1.25\,\mu$m on lane 2, $2.5\,\mu$m on lane 3, $5\,\mu$m on lane 4, $10\,\mu$m on lane 5 and $20\,\mu$m on lane 6. Thus the peaks of compounds 19 and 22 on lane 3 will be $250\,\mu$m apart; the compound 17 on lane 5 will be $100\,\mu$m and $250\,\mu$m apart from compounds 15 and 24, respectively. However, the three compounds 13, 21 and 23 will be co-eluted on lane 6 and will only be $40\,\mu$m and $60\,\mu$m apart from compounds 25 and 14, respectively. From the peak separation of the peptides shown in figure 9 it is clear that the separation of the peptides on lane 6 is not fully resolved. As discussed previously the system is designed for the separation of β-Amyloid binding peptides as reported by Cairo *et al*. [20] as well as potentially other β-Amyloid binding peptides, so far un-reported. None of the β-Amyloid binding peptides reported by Cairo *et al*. have dissociation constants of the range separable by lane 2. Thus the different peptides shown in table 1 will elute from each co-joining lane and reach the detection region (L_d) and either pass detectors or be absorbed onto the surface for analysis (possibly by mass spectrometry methods). It will be possible to explore further mixtures of peptides with unknown affinities and identify those with the optimal dissociation constant (K_d) values for interfering with β-Amyloid aggregation.

6. Discussion

The method presented provides a simple strategy for the design of microfluidic affinity chromatography systems, that removes the need for computationally expensive numerical simulations of the nonlinear governing equations. Such microfluidic affinity chromatography devices should be valuable for the separation of biomolecules (or classes of biomolecules) where specific receptors with high binding affinities are available. Such devices are envisaged to be of value for the quantification of a number of biomarkers from a complex mixture when integrated with an in-line detection systems, i.e. mass spectrometry. A limitation of microfluidic affinity chromatography systems is the low sample loading capacity. The maximal load concentration for a possible example, i.e. $H = 5\,\mu$m and $X_0 = 10^{-8}\,\text{mol}\,\text{m}^{-2}$, which fulfils $D_c \gg 1$ is $A_0 \approx 10\,\text{nM}$. Lab-on-a-chip dehvices offer the potential for handling small analyte samples and the incorporation of microfluidic affinity chromatography systems into such devices is crucial.

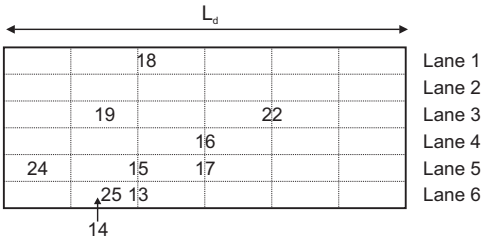

Figure 9: Schematic of the detection region showing the peak position of the peptides at the end of the total elution time. The compounds 21 and 23 are omitted as they are at the same location as compound 13 and the position of compound 14 is shown with an arrow as this elutes very close to compound 25. The vertical lines are only a guide for the eye and are $100\,\mu$m apart. (A schematic showing both the separation patches and the detection region is shown in figure 5.)

The incorporation of multiple receptor patches into one lane has several advantages and disadvantages. For instance, simple (single-patch) lanes are easier to fabricate but only useful if all the analytes can be separated by the same immobilised receptor molecule. This is rarely the case for biomolecules and thus the design strategy, reported here, allows mulitplex (multi-patch) lanes, incorporating multiple different receptor patches, to be designed for the separation of different classes of biomolecule analytes.

7. Conclusion

Two simple, analytical expressions, that describe the velocity and dispersion of analyte plugs in microfluidic affinity chromatography systems, are obtained from the analysis of the transport-reaction equations for microfluidic affinity systems for fast diffusion across the channel height and high adsorption capacity. These expressions are in good agreement with numerical simulations performed with the full 2D model and only depend on the global device parameters. Furthermore, these simple analytical expressions agree with the theory for column chromatography [23]. Together the two analytical expressions provide guidelines for the design of microfluidic affinity chromatography systems for the efficient separation of target molecules from sample mixtures. Conventionally, such a de-

sign would require computationally expensive numerical simulations of the nonlinear governing equations. However, the simple nature of the two analytical expressions allowed us to derive a design framework for the design of multiplex separation systems. In these designs more than one immobilised receptor patch and several parallel microfluidic lanes are incorporated into a microfluidic separation device providing the potential for separating a wide range of analytes.

References

[1] R. B. Schasfoort, Expert Review of Proteomics 1 (2004) 123–32.
[2] M. Pelzing, C. Neusüß, Electrophoresis 26 (2005) 2717–2728.
[3] D. Figeys, D. Pinto, Electrophoresis 22 (2001) 208–216.
[4] G. E. Yue, M. G. Roper, C. Balchunas, A. Pulsipher, J. J. Coon, J. Shabanowitz, D. F. Hunt, J. P. Landers, J. P. Ferrance, Analytica Chimica Acta 564 (2006) 116–122.
[5] B. E. Slentz, N. A. Penner, F. E. Regnier, Journal of Chromatography A 984 (2003) 97–107.
[6] Y. Liu, H. Lu, W. Zhong, P. Song, J. Kong, P. Yang, H. H. Girault, B. Liu, Analytical Chemistry 78 (2006) 801–808.
[7] S. L. S. Freire, A. R. Wheeler, Lab Chip 6 (2006) 1415–1423.
[8] F. Okanda, Z. E. Rassi, Electrophoresis 28 (2007) 89–98.
[9] Z. B. Stone, H. A. Stone, Physics of Fluids 17 (2005) –.
[10] W. C. Yang, X. H. Sun, T. Pan, A. T. Woolley, Electrophoresis 29 (2008) 3429–3435.
[11] J. Li, T. LeRiche, T. Tremblay, C. Wang, E. Bonneil, D. Harrison, P. Thibault, Molecular and Cellular Proteomics 1 (2002) 157–168.
[12] T. H. N. Nguyen, R. Pei, C. Qiu, J. Ju, M. Stojanovic, Q. Lin, Journal of Microelectromechanical Systems 18 (2009) 1198 – 1207.
[13] M. Zachariou, Affinity Chromatography: Methods and Protocols, Humana Press, New York, 2nd ed. edition, 2008.
[14] L. M. Braddick, P. J. Garland, M. F. Praeger, J. Butement, D. Friedrich, D. J. Morgan, T. Melvin, Analytical Biochemistry 424 (2012) 195 – 205.
[15] M. Ghosh, C. Alves, Z. Tong, K. Tettey, K. Konstantopoulos, K. J. Stebe, Langmuir 24 (2008) 8134–8142.
[16] L. Gonzalez-Macia, A. Morrin, M. R. Smyth, A. J. Killard, Analyst 135 (2010) 845–867.
[17] M. C. Peoples, H. T. Karnes, Journal of Chromatography B 866 (2008) 14 – 25.
[18] J. Pande, M. M. Szewczyk, A. K. Grover, Biotechnology Advances 28 (2010) 849 – 858.
[19] B. Yuan, P. Schulz, R. Liu, M. R. Sierks, Journal of Biotechnology 9 (2006) 171–175.
[20] C. W. Cairo, A. Strzelec, R. M. Murphy, L. L. Kiessling, Biochemistry 41 (2002) 8620–8629.
[21] H. J. de Haard, N. van Neer, A. Reurs, S. E. Hufton, R. C. Roovers, P. Henderikx, A. P. de Brune, J.-W. Arends, H. R. Hoogenboom, Journal of Biological Chemistry 274 (1999) 18218–18230.
[22] T. L. Hoffman, G. Canziani, L. Jia, J. Rucker, R. W. Doms, Proceedings of the National Academy of Sciences 97 (2000) 11215–11220.
[23] G. Guiochon, D. G. Shirazi, A. Felinger, A. M. Katti, Fundamentals of preparative and nonlinear chromatography, Academic Press, Boston, 2nd ed. edition, 2006.
[24] D. Friedrich, C. Please, T. Melvin, Sensors and Actuators B-Chemical 131 (2008) 323–332.
[25] D. A. Lauffenburger, J. J. Linderman, Receptors : models for binding, trafficking, and signalling, Oxford University Press, New York ; Oxford, 1993.
[26] A. Onell, K. Andersson, Journal of Molecular Recognition 18 (2005) 307–317.
[27] T. P. Burg, M. Godin, S. M. Knudsen, W. Shen, G. Carlson, J. S. Foster, K. Babcock, S. R. Manalis, Nature 446 (2007) 1066–1069.
[28] J. L. Schiff, The Laplace transform: theory and applications, Undergraduate texts in mathematics, Springer, New York, 1999.
[29] M. Abramowitz, Handbook of Mathematical Functions with Formulas, Graphs, and Mathematical Tables, John Wiley and Sons, 1972.
[30] J. H. Knox, M. T. Gilbert, Journal of Chromatography 186 (1979) 405–418.
[31] J. J. VanDeemter, F. J. Zuiderweg, A. Klinkenberg, Chemical Engineering Science 50 (1995) 3869–3882.
[32] G. I. Taylor, Proceedings of the Royal Society A 219 (1953) 186–203.